XVIII International Conference on Water Resources
CMWR 2010
J. Carrera (Ed)
CIMNE, Barcelona 2010

SPATIALLY ADAPTIVE FINITE ELEMENTS WITH TEMPORAL ADAPTION USING LOCAL TRUNCATION ERROR CONTROL FOR VARIABLY SATURATED FLOW

G.S. Yamoah[*], K.R. Fowler[*] and O. J. Eslinger[†]

[*] Clarkson University
Department of Mathematics, Potsdam, NY 13676-5815, USA
e-mail: yamoahgs@clarkson.edu, kfowler@clarkson.edu

[†] United States Army Corps of Engineers, ERDC
Vicksburg, MS 39180, USA
e-mail: owen.j.eslinger@usace.army.mil

Key words: Groundwater, temporal truncation error, spatial, adaption,

Summary. Variably saturated flow is often modeled with Richards' equation, a nonlinear partial differential equation. Obtaining robust numerical solutions efficiently continues to be challenging, in particular for infiltration into non-uniform porous media. In this work we present an *h*-adaptive Galerkin finite element method that coarsens and refines the mesh based on an a priori error indicator paired with a temporal adaption scheme that controls the local truncation error at each time step. The temporal scheme is based on linear extrapolation for smooth functions, but has been rigorously proven to work for nonsmooth problems when a finite-difference Jacobian is used. We present numerical results for the pressure head form of Richards' equation for infiltration problems into silt and clay, both of which lead to a nonsmooth model. We provide error and work measures to demonstrate the performance of the joint spatial-temporal adaption scheme when compared to a fixed grid approach with temporal error control, a fixed grid approach with heuristic time stepping, and a spatially adaptive approach with heuristic time stepping. We show that use of our joint scheme improves accuracy and computational efficiency.

1 INTRODUCTION

For this work, we focus on numerical solutions of Richards' equation (RE) as a model for flow in partially saturated porous media (Richards 1931). We propose a fully adaptive finite element method for robust, efficient solutions to the pressure-head form of RE and demonstrate the performance on infiltration into non-uniform porous media, which result in non-smooth partial differential equations.

1.1 Richards' equation

The pressure head form of RE in one spatial dimension is given by

$$S_s S_a(\psi)\frac{\partial \psi}{\partial t} + \eta \frac{\partial S_a(\psi)}{\partial t} = \frac{\partial}{\partial z}\left(K_s k_r(\psi)(1+\frac{\partial \psi}{\partial z})\right) \qquad (1)$$

where z is the vertical spatial dimension, S_s is the specific storage coefficient, η is the porosity of the media, K_s is the saturated hydraulic conductivity, and ψ is the pressure head. For this work, the nonlinear constitutive relations used to model the aqueous phase saturation, $S_a(\psi)$, and the relative permeability, $k_r(\psi)$ are the van Genuchten (Genuchten 1980) and Mualem (Mualem 1976) formulae given by

$$S_a(\psi) = \begin{cases} S_r + \dfrac{(1-S_r)}{[1+|\alpha\psi|^{\nu}]^m} & \psi < 0 \\ 1 & \text{otherwise} \end{cases} \qquad (2)$$

and

$$k_r(\psi) = \begin{cases} \dfrac{[1-|\alpha\psi|^{\nu-1}(1+|\alpha\psi|^{\nu})^{-m}]^2}{[1+|\alpha\psi|^{\nu}]^{m/2}} & \psi < 0 \\ 1 & \text{otherwise} \end{cases} . \qquad (3)$$

The parameter values are related to the mean pore size, α, and the uniformity of the pore-size distribution, ν. Here, S_r is the residual saturation and $m = 1 - 1/\nu$. The constitutive relations are nonlinear power functions which are computationally expensive to evaluate. In this work we use piecewise linear splines to reduce the cost during simulation. Note that for values of ν between 1 and 2 (such as those for silts and clays), the relations are not Lipschitz continuous much less differentiable at the water table, which occurs when saturated and unsaturated conditions exist in the domain.

1.2 Discretization

We denote the residual form of Richards' equation as

$$RE(\psi) = S_s S_a(\psi)\frac{\partial\psi}{\partial t} + \eta\frac{\partial S_a(\psi)}{\partial t} - \frac{\partial}{\partial z}\left(K_s k_r(\psi)(1+\frac{\partial\psi}{\partial z})\right) = 0. \qquad (4)$$

The weak form of RE is found by multiplying Eq. (4) by an appropriate weight function and integrating over time and space. We use the Galerkin method here with linear polynomials in space and piecewise constant in time, resulting in backward Euler temporal integration. Consider the space time domain $[a,b]\times[0,T]$ with initial condition $\psi(z,0) = \psi^0$ and boundary conditions $\psi(a,t) = \psi_a, \psi(b,t) = \psi_b$. Our finite element interpolation spaces are

$V_h = \{ v_h \mid v_h \in H^{1,h}([a,b]), v_h(a) = v_h(b) = 0 \}$,

$\hat{V}_h = \{ \hat{v}_h \mid \hat{v}_h \in H^{1,h}([a,b]), \hat{v}_h(a) = \psi_a, \hat{v}_h(b) = \psi_b \}$.

We formulate our problem as: given $\hat{\psi}^{n-1}$, find $\hat{\psi}^n$ such that $\int_{t^{n-1}}^{t^n}\int_a^b RE(\hat{\psi}^n)v_h\,dtdz = 0$ for all $\hat{\psi}^n \in \hat{V}_h, v_h \in V_h$. For this work, the resulting nonlinear system that arises at each time step is

solved with Newton's method using a finite difference Jacobian and an exact linear solve for the Newton step.

2 JOINT ADAPTION SCHEME

2.1 Temporal adaption

Since the solution of RE can involve the formation of a sharp wetting front that propagates through the domain, a significantly small time step may be required to capture the formation of the front but may not be needed for the entire simulation. Temporally adaptive methods for RE are often based on heuristics that grow or shrink the time step sized based on the internal iterative nonlinear and linear solvers. We consider a basic first-order adaptive method that controls the local truncation error at each step. These ideas are described in detail in (Kavanagh, et al. 2002) and proven to work on non-smooth problems when finite difference Jacobians are used (Fowler and Kelley 2005).

Our temporal error estimation makes use of $\hat{\psi}^{n-1}$ and $\hat{\psi}^{n-2}$ by approximation the local truncation error with

$$E_n = \left\|\hat{\psi}^n - \psi(z,t_n)\right\| \approx \frac{\Delta t_n^2}{2}\left\|\psi''(\xi_n)\right\|,$$

with $\left\|\psi''(\xi_n)\right\|$ approximated by $\left\|\psi''(\xi_n)\right\| \approx \dfrac{2\left\|\psi_{pre}^n - \hat{\psi}^n\right\|}{\Delta t_n(2\Delta t_n - \Delta t_{n-1})} = C_n$. Here the predictor is given by $\psi_{pre}^n = \hat{\psi}^{n-1} + \Delta t_n\left(\dfrac{\hat{\psi}^{n-1} - \hat{\psi}^{n-2}}{\Delta t_{n-1}}\right)$. The next time step is then computed using $\Delta t_{n+1} = \sqrt{\dfrac{2\cdot tol\cdot\varepsilon}{C_n}}$, where *tol* is a user specified tolerance to bound the local truncation error and $0<\varepsilon<1$ is chosen so that the truncation error satisfies $E_{n+1} \approx \dfrac{\Delta t_{n+1}^2}{2}C_n < tol$. For this work, if the truncation error is not below the tolerance, the current solution is rejected, the time step is decreased, and a new $\hat{\psi}^n$ is sought.

2.2 Spatial adaption

The spatial adaptive scheme is based on a finite element a priori error indicator given by $e \approx \sqrt{\left|\dfrac{\partial^2}{\partial z^2}\psi(z,t)\right|\Delta z^2/2}$ (Moaveni 2003). At each node z_k, the error is estimated using the approximation

$$e_k \approx \sqrt{\left| \frac{\dfrac{\psi_{k+1}^{n+1} - \psi_k^{n+1}}{\Delta z_k^{n+1}} - \dfrac{\psi_{k+2}^{n+1} - \psi_{k+1}^{n+1}}{\Delta z_{k+1}^{n+1}}}{\Delta z_k^{n+1} + \Delta z_{k+1}^{n+1}} \right| \frac{(\Delta z_k^{n+1} + \Delta z_{k+1}^{n+1})^{\,2}}{8}} \qquad (5)$$

and for each element $[z_k, z_{k+1}]$ of the mesh, the element error is the average of the error at its nodes.

The spatial adaption scheme is based on inserting and deleting nodes using Eq. (5) as a guide. Elements with low errors are merged and elements with large errors are split into two by inserting a node at the midpoint of the element. The coarsening procedure is done in the reverse order of the refinement process at the element level. That is, the newest nodes inserted during the refinement process are removed first. Moreover, the mesh cannot be coarsened beyond the initial mesh.

2.3 Fully adaptive approach

The joint adaption schemes proposed here combines the temporal and spatial adaption schemes described above. The user may specify whether or not spatial or temporal adaption is performed at each time step. The algorithm makes use of a spatial adaption flag and a temporal adaption flag, so the user has flexibility in the number of times each adaption process takes place. We outline the algorithm below; spatial adaption is performed first.

Spatial adaption phase

S1: Given $\hat{\psi}^{n-1}, \Delta t_{n-1}$

S2: Attempt to compute $\hat{\psi}^{n}$ on the current mesh, Ω_n

S3: If the nonlinear solver fails to converge, set $\Delta t_{n-1} = \Delta t_{n-1} / p_1$ and go to S2

S4: Using $\hat{\psi}^{n}$, compute and allocate all errors to elements along the mesh

S5: Use element errors to obtain the new mesh Ω_{n+1}

S6: Project $\hat{\psi}^{n-1}, \hat{\psi}^{n}$ onto Ω_{n+1}

S7: If maximum number of consecutive spatial adaption processes is reached, set spatial flag to NO, set temporal flag to YES and proceed to temporal adaption phase T1

S8: Go to S1

Temporal adaption phase

T1: Given $\hat{\psi}^{n-1}, \Delta t_{n-1}, \hat{\psi}^{n}, \Delta t_n$

T2: Attempt to compute $\hat{\psi}^{n+1}$ on Ω_{n+1} using Δt_n

T3: If the nonlinear solver fails to converge, set $\Delta t_n = \Delta t_n / p_1$ and go to T2

T4: Compute temporal error

T5: If $E_n > tol$, set $\Delta t_n = \Delta t_n / p_1$ and go to T2

T6: Compute Δt_{n+1}

T7: If maximum number of consecutive of temporal processes is met, set spatial flag to

YES and set temporal flag to NO.
T8: Go to T1

p_1 is a user specified constant. Sharp fronts which arise in the solution to RE occupy only a small portion of the domain, thus with the exception of the fronts, very few nodes are needed to produce acceptable levels of accuracy. We therefore begin our simulations with a very coarse mesh and a particularly small time step. Spatial adaption is used to determine the location of the front and then consecutive temporal adaption steps are used to determine the suitable step sizes thereafter. For the simulation results presented below, we started the adaption process with spatial adaption and then proceeded with 20 temporal adaption processes before adjusting the grid.

3 NUMERICAL RESULTS

We simulate flow through 10m long columns of silt and clay. Each simulation had constant head boundary condition of ($\psi(t,0) = 0.1$m) at the top and ($\psi(t,10) = 0$ m) at the bottom of the columns as well as hydrostatic equilibrium initial conditions, given by $\psi(0,z) = -z$ m. Extremly sharp fronts develop and propagate in the domain as a function of time requiring an initial time step of $\Delta t_0 = 10^{-6}$ (days). The model parameters of silt and clay are specified in (Kavanagh, et al. 2002). We compare results using four different approaches; the joint scheme (JNT), the spatial adaptive approach with heuristic time stepping (SPA/HS), a fixed spatial grid with heuristic time stepping (FG/HS), and a fixed grid with our temporal adaption scheme (FG/TA). The spatial grid was coarsened or refined based on $0.03 \le e_k \le 0.04$ and the temporal error tolerance requirement was $E_n < 0.01$.

For all four approaches, we begin each simulation with the same number of uniformly spaced nodes on the grid. Application of the spatial adaption process to the JNT and SPA/HS methods meant that the number of nodes varied at each time step. The simulations are repeated for initial uniformly spaced grids of different sizes for all four approaches.

The measure of error is the weighted L_1 norm obtained by comparing the solutions of the four approaches to that of the highly resolved grid and is given by

$$wL_1 = \frac{\sum_{i=1}^{N} \left| \psi_i^f - \psi_i \right| \Delta z_i}{\sum_{i=1}^{N} \Delta z_i}, \qquad (6)$$

where ψ_i^f and ψ_i are the values of the pressure head obtained at the elements of the highly resolved grid and our corresponding schemes respectively. Our measure of work includes the

number of time steps, the computational effort of the simulations, as well as the number of grid nodes.

The average time step sizes of the simulations are plotted against the average number of nodes for all four approaches for the clay and silt infiltrations in Figure 1. The plots show that the temporal adaption grows the time step sizes and overall, result in fewer time steps, and reduces the computational effort. That is the JNT and FG/TA methods, which make use of temporal adaption, require less work compared to the SPA/HS and FG/HS respectively

In Figure 2, the solution errors are plotted against the average number of nodes for all four approaches. The plots show that relatively low errors are obtained for the JNT and SPA/HS methods that make use of spatial adaption, even when initially very coarse grids are used. The uniformly fixed grid methods, FG/TA and FG/HS, on the other hand require fine grids to yield acceptably accurate results.

In Tables 1 and 2, we compare the results of the JNT and SPA/HS methods for the infiltrations in clay and silt in which the initial grids consist of 100 nodes, to those of the uniformly fixed grid methods, FG/TA and FG/HS, that use initial grids consisting of 401 nodes. The JNT and SPA/HS averaged about 115 nodes for the simulations. Again we see from the error columns of the two tables that the JNT and SPA/HS methods yeild more accurate results with fewer nodes compared to the two uniformly fixed grid approaches, FG/TA and FG/HS. Also in the tables, we demonstrated that the application of the temporal adaption scheme result in bigger time steps for the JNT and FG/TA approaches when compared to the heuristic time stepping schemes of the SPA/HS and FG/HS schemes respectively.

4 DISCUSSION AND CONCLUSIONS

We have presented a method for joint spatial and temporal adaption for Richards' equation and tested the method on infiltration problems for silt and clay media, both of which lead to non-Lipschitz saturation and permeability relations. Moreover, the infiltration setting leads to a non-smooth model at the water table. The joint scheme offers the user a chance to control the local temporal truncation error while the spatial adaption improves efficiency and accuracy. However, the spatial adaption scheme using heuristic time stepping is competitive and more work needs to be done to understand the relationships between the algorithm parameters and various solver and adaption tolerances.

WORKS CITED

Fowler, K.R., and C. T. Kelley. "Pseudotransient Continuation for Nonsmooth Nonlinear Equations." *SIAM Journal of Numerical Analysis* 43, no. 4 (2005): 1385-1406.

Genuchten, M.T. van. "A close-form equation for predicting the hydraulic conductivity of unsaturated soils." *Soil Sci. Soc. Am. J.*, 1980: 892-898.

Kavanagh, K.R., C. T. Kelley, C. Berger, J. Hallberg, and S. E. Howington. "Nonsmooth nonlinearities and temporal integration for Richards' equation." Edited by Ruud J. Schotting, W. G. Gray, and G. F. Pinder S. Majid Hassanizadeh. *XIV International Conference on Computational Methods in Water Resources.* 2002. 947-954.

Marsily, G. de. *Quantitative Hydrogeology.* San Diego, CA: Academic Press, 1986.

Moaveni, S. *Finite element analysis theory and applications with ANSYS.* Prentice Hall, 2003.

Mualem, Y. "A new model for predicting the hydraulic conductivity of unsaturated porous media." *Water Resources research* 12 (1976): 513-522.

Richards, L.A. "Capillary conduction of liquids through porous media." *Physics* 1 (1931): 318-333.

Figure 1: Comparison of the average temporal step size

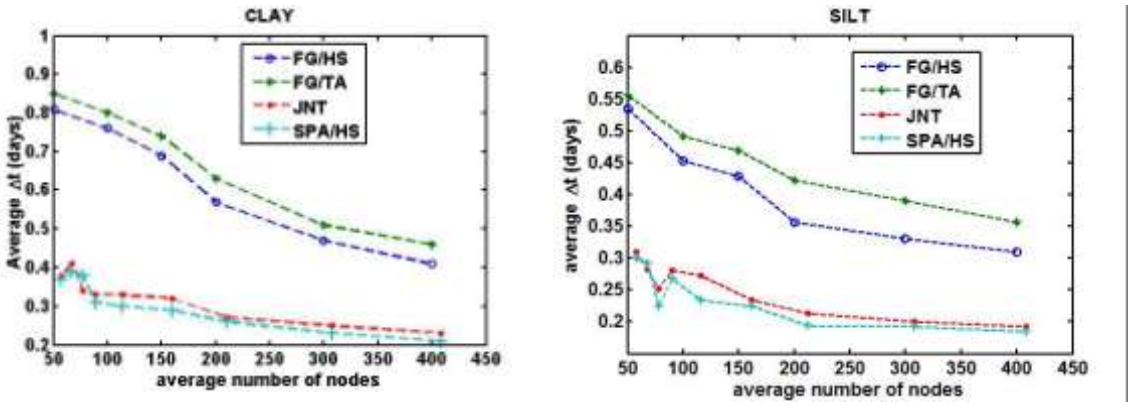

Figure 2: Error measurements

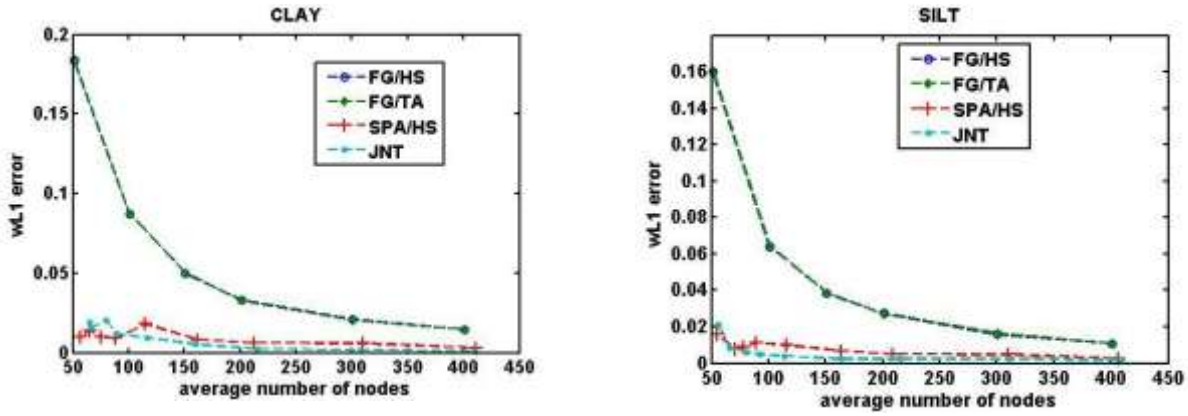

Table 1: CLAY

Method	Init. Nodes	Ave. Nodes	CPU time (s)	# of time steps	Ave Δt (days)	Error
JNT	101	114	67.704	111	0.272	9.372e-3
SPA/HS	101	116	84.986	121	0.234	1.607e-2
FG/TA	401	401	272.424	90	0.353	1.458e-2
FG/HS	401	401	312.676	97	0.312	1.467e-2

Table 2: SILT

Method	Init. Nodes	Ave. Nodes	CPU time (s)	# of time steps	Ave Δt (days)	Error
JNT	101	117	76.211	212	0.334	3.955e-3
SPA/HS	101	115	97.481	233	0.303	9.858e-3
FG/TA	401	401	161.511	155	0.452	1.091e-2
FG/HS	401	401	219.358	170	0.413	1.089e-2